Environ. Sci. Technol. **1998**, *32,* 760−765

Identification of the Nickel Uranyl Phosphate Deposits on *Citrobacter* sp. Cells by Electron Microscopy with Electron Probe X-ray Microanalysis and by Proton-Induced X-ray Emission Analysis

GABRIELA BASNAKOVA,[†] ANTHONY J. SPENCER,[‡] EVA PALSGARD,[§] GEOFF W. GRIME,[§] AND LYNNE E. MACASKIE*,[†]

School of Biological Sciences, The University of Birmingham, Edgbaston, Birmingham B15 2TT, U.K., Department of Physiology, Medical School, The University of Birmingham, Edgbaston, Birmingham B15 2TT, U.K., SPM Unit, Department of Nuclear Physics, The University of Oxford, Keble Road, Oxford OX1 3RH, U.K.

Immobilized cells of a *Citrobacter* sp. can remove heavy metals from wastewaters by deposition of metals with enzymatically liberated phosphate. Nickel is not removed effectively by this technique, but Ni^{2+} can be intercalated into cell-bound, crystalline HUO_2PO_4 previously deposited enzymatically. This technique for efficient removal of Ni from solution has been generically termed microbially enhanced chemisorption of heavy metals (MECHM). The nickel uranyl phosphate deposits bound to *Citrobacter* sp. cells immobilized in polyacrylamide gel (PAG) were analyzed using scanning transmission electron microscopy with electron probe X-ray microanalysis (EPXMA) and proton-induced X-ray emission analysis (PIXE). Both methods gave the molar ratios of nickel, uranium, and phosphorus in the deposits as close to 1:2:2 in all analyzed parts of the sample. EPXMA proved that the deposits were localized on the surface of cells inside PAG particles as well as those immobilized on the edge. Small deposits of nickel uranyl phosphate were also found in PAG between the cells, indicating the possible involvement of extracellular polymeric substances (EPS) in the creation of intercellular deposits. These findings confirm the mechanism of MECHM and show that this mechanism operates throughout the immobilized cell matrix. The use of two independent methods of solid-state analysis in a common sample provides validation of both techniques for the spatial and quantitative analysis of biomass-bound elements.

Introduction

Microbially enhanced chemisorption of heavy metals (MECHM) is a new, effective method for the removal of some heavy metals that are resistant toward direct removal from dilute aqueous solutions (*1*−*3*). It comprises enzymatically enhanced biomineralization of a suitable metal (priming metal) in the form of an insoluble polycrystalline metal hydrogen phosphate on a microbial cell surface, followed by incorporation of a second metal (target metal) into the priming layer, which effectively comprises a bio-inorganic ion exchanger. Formation of metal hydrogen phosphate on bacterial cell surfaces has been described using *Acinetobacter* sp. (*4*), *Citrobacter* sp. (*5*−*7*), and also *Escherichia coli* containing the cloned gene *phoN* (*8*) that encodes a phosphatase activity responsible for metal bioprecipitation via production of phosphate ligand (P_i), which precipitates with metal cations at the microbial cell surface (*5*−*9*). This activity, naturally expressed and persisting in nongrowing biomass of *Citrobacter* sp., enables continuous removal of metals from aqueous flows presented to polyacrylamide gel (PAG)-immobilized cells within flow-through columns and cumulative deposition of metal phosphate upon the immobilized biomass. In the case of uranyl ion, biomineralization of UO_2^{2+} by enzymatically (phosphatase)-liberated P_i gave cell-bound polycrystalline hydrogen uranyl phosphate (HUO_2PO_4) (*5*), the identity and crystallinity of which were confirmed by the combined use of electron probe X-ray microanalysis (EPXMA; also known as energy-dispersive X-ray analysis, EDAX), solid-state infrared spectroscopy, X-ray powder diffraction (XRD) analysis, and magic angle spinning nuclear magnetic resonance (*5, 10*). The material was accumulated on the cell surface as polycrystalline, needlelike deposits (*5*), co-localized with the *Citrobacter* phosphatase by immunogold labeling (*11, 12*). The enzyme was found in two "pools", one in the periplasmic space (*11*) and one extracellularly, within the matrix of an extracellular polymeric substance (EPS) (*12*).

In contrast to UO_2^{2+}, Ni^{2+} was not accumulated by this method, despite the high insolubility of nickel phosphate (*1*). The resistance of Ni^{2+} to bioremediation was noted also by other authors (*13*). However, the primary cellular deposit of HUO_2PO_4 promoted accumulation of Ni in the form of nickel uranyl phosphate ($Ni(UO_2PO_4)_2$) and removal of Ni from solution (*1*−*3*).

The importance of microbial templates in biomineralization has been recognized, and cases of "bio-creation" of polycrystalline layered sediments have been reported (*14, 15*). The concept of MECHM was proposed on the basis of the highly regular layered crystal structure of both chemically (*16, 17*) and microbially (*1*) created HUO_2PO_4. A high mobility of protons in the interlamellar space of "chemical" HUO_2PO_4 (*16*) confers an intercalative ion-exchange property (*17*) responsible for the subsequent nickel accumulation as $Ni(UO_2PO_4)_2$:

$$2HUO_2PO_4 + Ni^{2+} \rightarrow Ni(UO_2PO_4)_2 + 2H^+$$

X-ray powder diffraction analysis (XRD) identified nickel-saturated biomass-bound hydrogen uranyl phosphate as $Ni(UO_2PO_4)_2 \cdot 7H_2O$ (*1, 3*). Comparison of the *a*, *b*, and *c* crystallographic cell dimensions of the $Ni(UO_2PO_4)_2$ deposits with those of the original HUO_2PO_4 proved intercalation of nickel into the layered HUO_2PO_4 structure and function of this as an ion-exchange material. These studies used PAG-immobilized cells to demonstrate the potential application of MECHM to aqueous waste remediation, but no information was obtained regarding penetration of Ni^{2+} or distribution of the $Ni(UO_2PO_4)_2$ deposits throughout the PAG matrix. Such spatial information can only be gained by direct imaging methods. The relative efficiencies in MECHM of the cells

* Corresponding author telephone: (0044)121-414-5889; fax: (0044)121-414-6557; e-mail: L.E.Macaskie@bham.ac.uk.
[†] School of Biological Sciences, The University of Birmingham.
[‡] Medical School, The University of Birmingham.
[§] Department of Nuclear Physics, The University of Oxford.

S0013-936X(97)00555-5 CCC: $15.00
Published on Web 01/27/1998

TABLE 1. Samples Taken for Study

sample	type of deposit[a]	Ni challenge of the column[b]	regeneration of the column[c]
I	HUO_2PO_4		
II	$Ni(UO_2PO_4)_2$	first	
III	$Ni(UO_2PO_4)_2$	second	citrate buffer
IV	$Ni(UO_2PO_4)_2$	second	priming soln

[a] Deposit on *Citrobacter* cells immobilized in shredded PAG. [b] Column with HUO_2PO_4 deposit was challenged with 1 mM $Ni(NO_3)_2$ (aqueous solution). [c] Column loaded with the $Ni(UO_2PO_4)_2$ deposit was regenerated by washing with 2 mM citrate buffer (pH 7) or with "priming solution" [20 mM MOPS/NaOH buffer, 2 mM citrate buffer, 5 mM glycerol-2-phosphate (G2P, phosphatase substrate and phosphate donor for enzymatically mediated HUO_2PO_4 formation), 1 mM $UO_2(NO_3)_2$, pH 7] and submitted to a second challenge with 1 mM $Ni(NO_3)_2$ solution. Original data are in ref 3.

immobilized within the PAG matrix and those immobilized on its edge would be subject to the diffusion of phosphate donor molecule and uranyl ion into the gel during "priming" and diffusion of Ni^{2+} (inward) and protons (outward) during subsequent ion exchange. Proton liberation (above) has implications for the localized pH. Phosphatase activity was reduced at pH values of less than 5.0 (*6*) and metal phosphates are more soluble (*18*), having implications for prolonged application and the participation of cells deep within the gel.

The aim of this investigation is to establish the proportion of immobilized cells that participate in MECHM via determination of the elemental topography of gel-immobilized cells loaded with HUO_2PO_4 or $Ni(UO_2PO_4)_2$. Such information is necessary for optimization of the technology. The bioremediation of uranium-contaminated drainage water from the ENUSA mining facility (Spain) was successfully demonstrated (*19, 20*), and the use of MECHM for the remediation of nickel wastes using the solid HUO_2PO_4 from this primary process represents also a use for the recovered U. This study describes the application of scanning transmission electron microscopy (STEM) in conjunction with electron probe X-ray microanalysis (EPXMA) (*21*) of intact specimens prepared from cryofixed samples by cryoultramicrotomy. Concurrent elemental mapping and quantitative analysis of the same intact specimens by proton-induced X-ray emission (PIXE) (*22*) is novel and provides a complementary approach to confirm the elemental composition and spatial distribution within the PAG matrix, which is discussed in relation to the potential for gel-immobilization systems for MECHM.

Materials and Methods

Samples of *Citrobacter* sp. Cells Loaded with HUP and NiUP Deposits. Samples from columns operating MECHM and containing HUO_2PO_4 or $Ni(UO_2PO_4)_2$ deposits on *Citrobacter* cells immobilized in PAG were obtained as described previously (*2, 3*). *Citrobacter* cells (1 g wet weight) were immobilized in 10 g of PAG. The gel was shredded through an 8-mesh sieve, providing extrusions (particles) of diameter <1.3 mm and length approximately 60−80 mm. Shredded gels (10 g) were held within columns (22 mm i.d. × 8 cm, fluid volume 20 mL) used as flow-through reactors (*2, 3*). Representative samples of PAG particles loaded with HUO_2PO_4 or $Ni(UO_2PO_4)_2$ deposit were taken from the middle of each column and used without further treatment for preparation of cryosections for analysis (see below). The samples studied are summarized in Table 1. All samples were taken from at least two independent experiments, using columns prepared from cells pregrown in separate batches.

Examination of the PAG-Immobilized Cells Using Electron Microscopy and EPXMA. Selected specimen areas with *Citrobacter* cells immobilized both inside and at the edge of the PAG matrix were examined by electron microscopy and analyzed by EPXMA and PIXE (below) as appropriate for uranium, phosphorus, and nickel.

EPXMA is a well-established technique for quantitative analysis of elemental composition at high spatial resolution (*21*). No stains or chemical fixatives were used during specimen preparation. To minimize ice crystal formation in frozen samples, a 1−2 mm length of the PAG-immobilized cells was cut from the shredded particles. Pieces were mounted onto aluminum specimen holders (Leica, U.K.) using tissue tek low-temperature adhesive (Leica, U.K.), plunge-frozen in liquid propane cooled by liquid nitrogen, using a Reichert KF80 cryofixation device (Leica, U.K.) and stored in liquid nitrogen for cryoultramicrotomy. Cryosections (300 nm thick) were cut across the diameter of the frozen samples with a Reichert FC4/Ultracut E cryoultramicrotome (Leica UK) at a sectioning temperature of 173 K, using dry glass knives. A set of random cryosections was prepared, which contained multiple cases of the cell-bound deposits both on the edge and deep inside the shredded PAG particles, so that whole cross-section area was sampled in each case (due to cold shrinking and compression when cut, the actual diameter of PAG particles was less than 600 μm). Sections were mounted onto Formvar-coated 75 mesh Ti grids, sandwiched, and pressed under a second grid; the two grids were separated within the cryochamber before freeze-drying at a temperature of 193 K overnight. Sections were stored under desiccating conditions before analysis.

Sections were observed and analyzed in a JEOL 100CX II electron microscope (accelerating voltage 100 kV), fitted with a high-resolution scanning attachment, LaB_6 filament, 30 mm^2 Si(Li) ATW detector, and an Oxford Instruments Link ISIS microanalysis system. With the electron microscope operating in scanning transmission mode, X-ray spectra of different cryosections were obtained from deposits at the original edge of the PAG ("edge", arrowed in Figure 1a,b), from deposits on bacterial cell surfaces within the PAG ("bacteria", arrowed in Figure 1a,b), and for sample II from the small granules (arrowed in Figure 1c). As a background control, a tissue tek area of sample I was analyzed in the same way. Spectra were obtained for 200 s lifetime per spectrum, with a probe current of 0.5−1.5 nA.

X-ray spectra were quantified using the Oxford Instruments Link ISIS Bioquant program. Each spectrum was corrected for the contribution of the grid and film to the background continuum. Quantitation of elemental content for P, Ni, and U (in terms of mmol/kg dry weight of biomass) was performed with reference to bovine serum albumin/inorganic salt standards (*23*). Data are expressed as molar ratios of phosphorus to uranium (P/U), phosphorus to nickel (P/Ni), and uranium to nickel (U/Ni) for each area analyzed. The correlation between elements in each area was also calculated.

Examination of the PAG-Immobilized Cells by PIXE Microanalysis. Quantitative elemental analyses of the same cryosections as used for electron microscopy and EPXMA were done using the Oxford scanning proton microprobe (*22, 24, 25*). Each cryosection on a Ti grid was fixed onto an aluminum holder and held within a 3-MeV proton beam. By using different magnification, suitable areas of the cryosections were chosen and elemental maps (50 × 50 μm) were obtained. Subsequently, point analyses were run within each elemental map (3−6 points), and the data obtained were statistically evaluated, summarizing the data from the same types of cryosection areas (deposits on the edge of the PAG and the deposits inside PAG cryosections) so that direct comparison with the data from EPXMA analyses was possible. The data were corrected to give elemental composition using simultaneously determined Rutherford back-scattering (RBS) spectra, as described previously (*6, 26*).

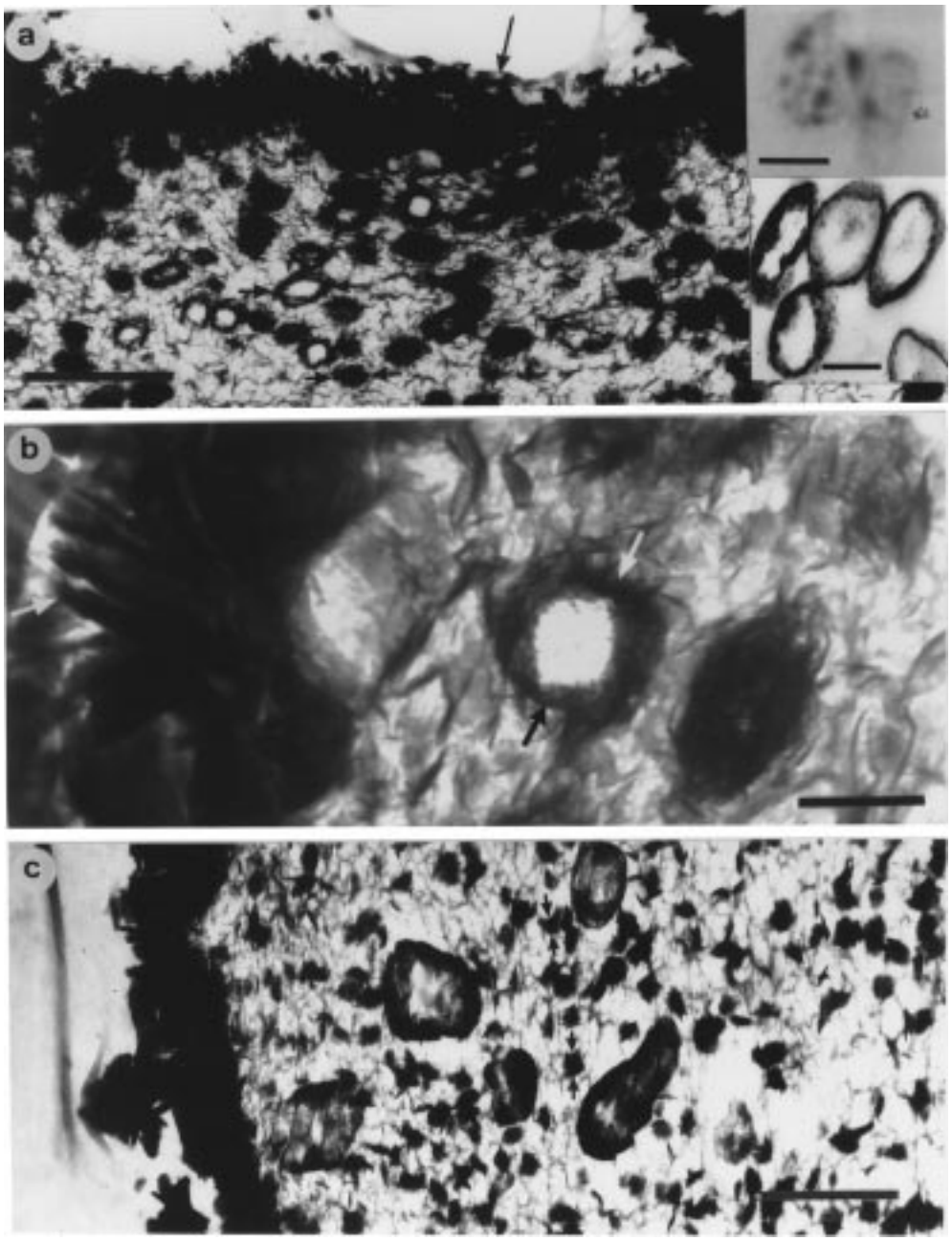

FIGURE 1. (a) Electron micrograph (scale bar 5 μm) of a cryosection of sample III. *Citrobacter* cells are entrapped in PAG matrix and covered with an electron opaque deposit of $Ni(UO_2PO_4)_2$, which is bound to cell surfaces and present at higher concentration on an edge of the PAG matrix ("edge" and "bacteria" are arrowed). Inset micrographs are sections of free *Citrobacter* cells without (top; scale bar 0.9 μm) and with HUO_2PO_4 deposit (bottom; scale bar 0.4 μm) (non-cryosections made by standard techniques; details in ref 11). (b) Electron micrograph (scale bar 1 μm) of a cryosection of sample III (expanded area of panel a, center of field). The polycrystalline character of the $Ni(UO_2PO_4)_2$ deposit on the edge of the PAG matrix (left) and on the surface of a sectioned cell (central) is clearly seen. No intracellular deposit is seen in the sectioned cell (cf. panel a inset, bottom). (c) Electron micrograph (scale bar 1 μm) of a cryosection of sample II. Extracellular granules of $Ni(UO_2PO_4)_2$ deposit (arrowed), smaller than immobilized cells, are seen throughout the whole section.

Results and Discussion

Initial attempts to employ standard scanning electron microscopy or transmission electron microscopy techniques gave poor resolution of the cells and/or related deposits (Basnakova, G., and Spencer, A. J., unpublished). Electron microscopy of ultrathin cryosections of shredded PAG particles containing *Citrobacter* with $HUO_2PO_4/Ni(UO_2PO_4)_2$ deposits was used to provide information about the distribution of the electron opaque material (Figure 1). Solid deposits are visible in association with *Citrobacter* cells immobilized throughout the PAG matrix, with a higher concentration of deposit on the matrix edge than on cells within. The total gel depth shown in Figure 1a was ca. 13 μm (distance from edge to center of gel particles was approximately 300 μm). A complete depth profile was also done (see below). Sectioned immobilized cells (arrowed, Figure 1b) show no intracellular deposit in accordance with the surface localization of HUO_2PO_4 (Figure 1a, inset, see also refs 11 and 12). The pattern of HUO_2PO_4 deposition was similar in immobilized (Figure 1a, b) and free cells (Figure 1a, inset, bottom) ruling out artifacts introduced during preparation. Uranyl-unchallenged cells had no electron opaque deposit (Figure 1a, inset, top). In addition to the cell-bound deposits, extracellular granules of subcellular size

TABLE 2. Analysis of Sections Using EPXMA

sample	deposit[a]	n[b]	P/U molar ratio[c] (correlation[d])	P/Ni molar ratio (correlation)	U/Ni molar ratio (correlation)
I	bacteria	30	1.006 ± 0.052 (0.97)		
I	edge	10	0.976 ± 0.030 (0.92)		
II	bacteria	30	1.043 ± 0.058 (0.90)	2.242 ± 0.098 (0.94)	2.154 ± 0.862 (0.94)
II	edge	10	0.948 ± 0.027 (1.00)	2.063 ± 0.100 (1.00)	2.174 ± 0.061 (1.00)
II	small granules	10	1.014 ± 0.030 (0.96)	2.259 ± 0.123 (0.82)	2.229 ± 0.118 (0.83)
III	bacteria	30	0.953 ± 0.064 (0.99)	2.004 ± 0.208 (0.99)	2.104 ± 0.162 (1.00)
III	edge	10	0.911 ± 0.089 (1.00)	1.889 ± 0.288 (1.00)	2.067 ± 0.148 (1.00)
IV	bacteria	30	1.008 ± 0.079 (0.97)	2.201 ± 0.202 (0.97)	2.185 ± 0.141 (0.97)
IV	edge	10	0.961 ± 0.035 (0.97)	2.158 ± 0.183 (0.85)	2.246 ± 0.167 (0.90)

[a] Area of cryosection analyzed: bacteria, deposits on cell surfaces inside PAG matrix; edge, edge of shredded PAG with immobilized *Citrobacter* cells; small granules, discrete extracellular granules. See Figure 1. [b] n = number of independent regions analyzed. [c] Ratio of elemental content for given elements in analyzed region; data are given as mean ± standard deviation. [d] Correlation coefficient (r^2) for each pair of elements for the value of n shown.

TABLE 3. Analysis of Sections Using PIXE

sample	area[a]	n[b]	P/U molar ratio[c]	P/Ni molar ratio	U/Ni molar ratio
I	map	3	0.880 ± 0.021		
I	inside area	4	0.904 ± 0.121		
II	edge	5	0.965 ± 0.025	2.019 ± 0.082	2.090 ± 0.079
II	inside area	5	0.876 ± 0.091	1.916 ± 0.226	2.192 ± 0.104
III	map	3	1.075 ± 0.133	2.042 ± 0.060	1.919 ± 0.201
III	edge	2	1.004 ± 0.224	1.849 ± 0.328	1.853 ± 0.088
III	inside area	5	1.117 ± 0.155	2.071 ± 0.086	1.920 ± 0.151
IV	map	3	0.964 ± 0.058	1.856 ± 0.032	1.890 ± 0.183
IV	edge	16	1.012 ± 0.122	2.030 ± 0.175	1.974 ± 0.189
IV	inside area	2	0.863 ± 0.075	1.965 ± 0.308	2.271 ± 0.159

[a] Area of cryosection analyzed: map, chosen area of size 50 × 50 μm, analyzed in a "scanning" manner and providing an average elemental composition; edge, edge area of shredded PAG with immobilized *Citrobacter* cells; inside area, area of cryosection inside shredded PAG with *Citrobacter* cells (other than edge). [b] Number of the map-type analyses (50 μm × 50 μm) or independent point analyses within a particular area analyzed. [c] Molar ratio of element content for given elements in analyzed area; data are given as mean ± standard deviation.

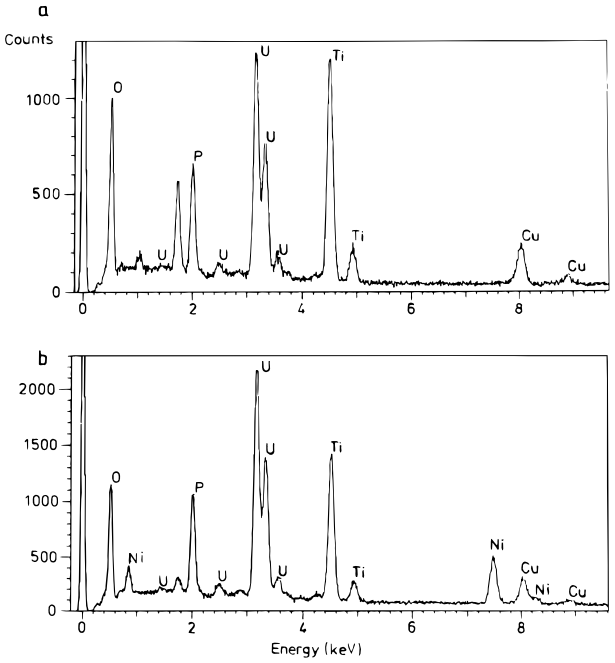

FIGURE 2. EPXMA spectrum of cryosection of part of a single *Citrobacter* cell immobilized in PAG and loaded with (a) HUO_2PO_4 (sample I) and (b) $Ni(UO_2PO_4)_2$ (sample II). Ti is from the EM grid.

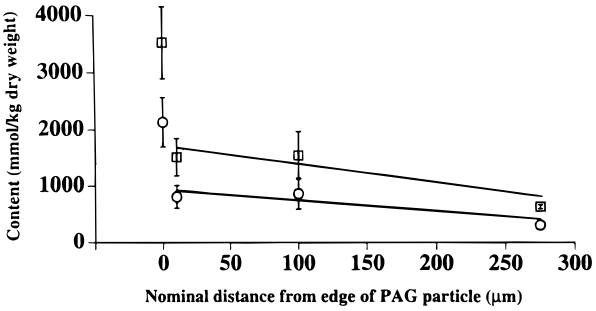

FIGURE 3. Change in elemental content of cryosections of sample II with distance from the edge of the PAG particle. The diameter of PAG particles after preparation of cryosections was less than 600 μm (cold shrinking and cutting compression); therefore, the change in elemental content is representative for half of the diameter of a PAG particle. The nominal distance of 300 μm corresponds to the central point of the complete gel section. (□) Content of P; (○) content of Ni. U was similar to P and is not shown.

and of the same appearance as the cell-bound electron opaque material are clearly seen distributed throughout the samples (Figure 1c, arrowed).

To establish the identity of the deposits and to prove unequivocally an involvement of immobilized cells throughout the gel in metal uptake, representative areas of these samples were taken throughout the areas of cryosections, and multiple EPXMA measurements on the content of phosphorus, uranium, and nickel were made. The EPXMA spectra of HUO_2PO_4 (sample I) and $Ni(UO_2PO_4)_2$ (sample II) deposits (identity of bulk preparations confirmed by XRD as described previously (*3*)) are shown in Figure 2. From these spectra and according to the method of Warley (*23*), the X-ray emission intensities of the elements were expressed as the mean molar ratio of a particular pair of elements (Table 2). As controls, electron transparent regions were tested. Here, the P, U, and Ni content was negligible. Nickel was not found in any significant amount in sample I (HUO_2PO_4 deposits). From Table 2, it is concluded that the molar ratios of the

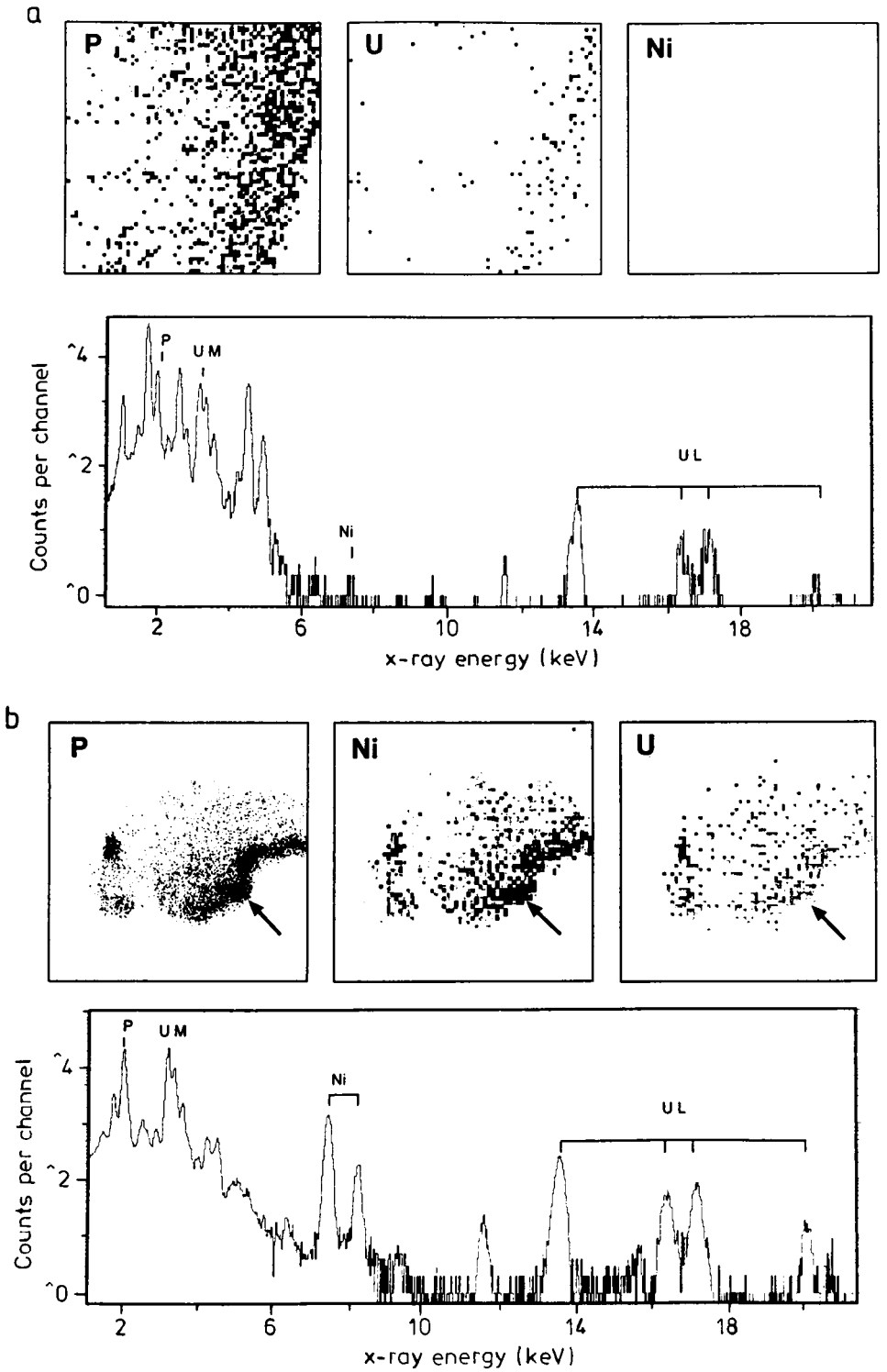

FIGURE 4. PIXE "elemental maps" (50 × 50 μm scan area) and spectra of *Citrobacter* cells immobilized in PAG and loaded with (a) HUO_2PO_4 (sample I) and (b) $Ni(UO_2PO_4)_2$ (sample II). UM and UL distinguishes L and M lines of uranium. Arrowed: edge area corresponding to the edge seen in Figure 1a.

elements correspond to the molar composition of HUO_2PO_4 (P/U = 1) or $Ni(UO_2PO_4)_2$ (P/U = 1, P/Ni = 2, U/Ni = 2) as appropriate. The small standard deviations and high correlation coefficients show that the composition of the deposits was consistent throughout the analyzed areas. Samples at or near the edge of the PAG matrix had a higher overall concentration of elements than those near the center, but there were no significant differences in the composition when expressed as elemental concentrations in the edge deposits and in the bacteria deposits inside the PAG matrix (Figure 3). This demonstrates that MECHM occurs both on the edge and inside of the matrix, but the process within is less extensive, probably attributable to diffusional limitations for glycerol-2-phosphate and uranium inside the matrix particles. There was little difference in metal loading in cells 10 μm within the particle and those at the center (Figure 3). The results in Table 2 also show that the $Ni(UO_2PO_4)_2$ deposits created from the "new" HUO_2PO_4 (first Ni^{2+} challenge, sample II) and those created from a "regenerated" HUO_2PO_4 column (unloading of Ni^{2+}, followed by a second Ni^{2+} challenge,

samples III and IV) have the same composition, as indicated by previous studies using XRD (*3*). Extracellular granules (Figure 1c, arrowed) comprised $Ni(UO_2PO_4)_2$ as with the other Ni-loaded HUO_2PO_4 deposits. This finding can be related to a recent report that an extracellular polymeric substance (EPS) of *Citrobacter* O16 was identified as a polysaccharide with 3.3% of phosphorus in a form of glycerol phosphate (*27*). The presence of polymer-associated extracellular phosphate in juxtaposition to EPS-localized extracellular phosphatase in the present *Citrobacter* (*12*) can clearly be envisaged as a creator of nucleation foci for subsequent biomineralization, both at the cell surface and in the intercellular spaces of the PAG matrix. Accordingly, other studies on the accumulation of Ag^+ by free cells of *Citrobacter* have shown, using atomic force microscopy, the presence of "tethered" crystals of Ag_3PO_4 linked to the cells via fibrils of EPS (*12*).

PIXE analysis (*22*) was employed to confirm the data obtained by EPXMA using the same samples. The proton beam used for PIXE analysis in this work provided a maximum spatial resolution of 1 μm, which was less than that obtained by EPXMA (up to 0.02 μm) but was sufficient for differentiation between deposits on the edge of the PAG matrix and those localized within (*22*). The low scattering and long penetrating power of MeV protons (typically 100 μm in organic samples) means that, unlike EPXMA, the spatial resolution is maintained even in thick samples (*22*), but this advantage was not exploited with these thin sections. Three types of analyses were performed. First, small (50×50 μm) square sample areas (elemental maps) were produced, and their complete areas were analyzed in the scanning manner providing an average elemental composition of the whole particular "map". Examples of PIXE spectra and elemental maps for areas of HUO_2PO_4-loaded (I) and $Ni(UO_2PO_4)_2$-loaded samples (II) are shown in Figure 4. Three areas were chosen and analyzed in each of the samples I−IV (Table 1). An edge area of the shredded PAG matrix with clearly visible deposits corresponding to the edge in EPXMA (see above) was analyzed at several different points. Similarly, the inside area of the shredded PAG matrix with clearly visible deposits was analyzed. Because of the lower spatial resolution of the PIXE method (see above), point analyses of the inside areas in some cases probably covered also extracellular granules close to the cell-bound deposits, revealed by electron microscopy. Therefore, elemental analyses of the deposits in the inside areas can be considered as corresponding to both bacteria and extracellular granules in the same samples analyzed by EPXMA. Multiple point analyses of the edge areas and inside areas were done for each sample (I−IV), and their statistical evaluation, employing program GUPIX (*28, 29*), is summarized and presented together with similar evaluation of the elemental maps analyses, in Table 3. The elemental compositions are presented as the mean molar ratio for a particular pair of elements together with the standard deviation. The molar ratios of the elements obtained from the PIXE analyses again correspond to the molar composition of HUO_2PO_4 (P/U = 1) or $Ni(UO_2PO_4)_2$ (P/U = 1, P/Ni = 2, U/Ni = 2) and thus unequivocally confirm the findings from the corresponding EPXMA analyses.

The combination of EPXMA and PIXE microanalysis proved to be an efficient and accurate approach for obtaining direct spatial information about microbial cells immobilized within a PAG matrix and provided a better understanding of the processes of biomineralization and of MECHM. Although PAG is too toxic for use in wastewater treatment process, this study demonstrates that in principle gel-immobilization systems would be appropriate for this purpose. Despite an approximate 2.5-fold concentration of the metals at the edge of the gel particles, the transects reveal penetration of the metals to all cells within the gel. Furthermore, efficient operation of MECHM is confirmed by the conservation of elemental ratios throughout the gel.

Acknowledgments

The authors thank the BBSRC Chemicals and Pharmaceuticals Directorate for financial support (ROPA Award Grant PAC 6/2677). Use of the *Citrobacter* strain N14 was by kind permission of ISIS Innovation, Oxford, U.K., under license.

Literature Cited

(1) Bonthrone, K. M.; Basnakova, G.; Lin, F.; Macaskie, L. E. *Nat. Biotechnol.* **1996**, *14*, 635.

(2) Basnakova, G.; Macaskie, L. E. *Biotechnol. Lett.* **1996**, *18*, 257.

(3) Basnakova, G.; Macaskie, L. E. *Biotechnol. Bioeng.* **1997**, *54*, 319.

(4) Dick, R. E.; Boswell, C. D.; Macaskie, L. E. *Proceedings of the International Conference on Biohydrometallurgical Processing*; University of Chile: Vina del Mar, Chile, 1995; p 177.

(5) Macaskie, L. E.; Empson, R. M.; Cheetham, A. K.; Grey, C. P.; Skarnulis, A. J. *Science* **1992**, *257*, 782.

(6) Tolley, M. R.; Strachan, L. F.; Macaskie, L. E. *J. Ind. Microbiol.* **1995**, *14*, 271.

(7) Macaskie, L. E. *J. Chem. Technol. Biotechnol.* **1990**, *49*, 357.

(8) Basnakova, G.; Stephens, E. R.; Macaskie, L. E. Unpublished results.

(9) Macaskie, L. E.; Bonthrone, K. M.; Rouch, D. A. *FEMS Microbiol. Lett.* **1994**, *121*, 141.

(10) Yong, P.; Macaskie, L. E. *J. Chem. Technol. Biotechnol.* **1995**, *63*, 101.

(11) Jeong, B. C.; Hawes, C.; Bonthrone, K. M.; Macaskie, L. E. *Microbiology* **1997**, *143*, 2497.

(12) Bonthrone, K. M.; Macaskie, L. E. In *Modeling of genetic, biochemical, cellular and microenvironmental parameters determining bacterial sorption and mineralization processes for recuperation of heavy or precious metals*; Final Report, EC Contract BR2/0199/C, Project No. BE-5350, Brussels, Belgium, 1995; p 86.

(13) Tsezos, M.; Remoudaki, E.; Angelatou, V. *Int. Biodeterior. Biodegrad.* **1995**, *35*, 129.

(14) Mann, S. *Chem. Ind.* **1995**, 93.

(15) Mann, S.; Ozin, G. A. *Nature* **1996**, *382*, 313.

(16) Pham-Thi, M.; Colomban, P. *Solid State Ionics* **1985**, *17*, 295.

(17) Clearfield, A. *Chem. Rev. (Washington, D.C.)* **1988**, *88*, 125.

(18) Dean, J. A. *Langes's Handbook of Chemistry*, 14th ed.; Mc Graw-Hill, Inc.: New York, 1992.

(19) Macaskie, L. E.; Lloyd, J. R.; Thomas, R. A. P.; Tolley, M. R. *Nucl. Energy* **1996**, *35*, 257.

(20) Macaskie, L. E.; Yong, P.; Doyle, T. C.; Roig, M. G.; Diaz, M.; Manzano, T. *Biotechnol. Bioeng.* **1997**, *53*, 100.

(21) Spencer, A. J.; LeFurgey, A.; Ingram, P.; Mandel, L. J. *J. Am. Soc. Nephrol.* **1991**, *1*, 1321.

(22) Breese, M. B. H.; Grime, G. W.; Watt, F. *Annu. Rev. Nucl. Part. Sci.* **1992**, *42*, 1.

(23) Warley, A. *J. Microsc.* **1990**, *157*, 135.

(24) Grime, G. W., Dawson, M.; Marsh, M.; McArthur, I. C.; Watt, F. *Nucl. Instrum. Methods* **1991**, *B54*, 52.

(25) Johannson, S. A. E.; Campbell, J. L. *PIXE—a novel technique for elemental analysis*; Wiley: Chichester, UK, 1988.

(26) Yong, P.; Macaskie, L. E. *J. Chem. Technol. Biotechnol.* **1995**, *63*, 101.

(27) Kocharova, N. A.; Thomas-Oates, J. E.; Knirel, Y. A.; Shashkov, A. S.; Dabrowski, U.; Kochetkov, N. K.; Stanislavsky, E. S.; Kholodkova, E. V. *Eur. J. Biochem.* **1994**, *219*, 653.

(28) Maxwell, J. A.; Campbell, J. L.; Teesdale, W. J. *Nucl. Instrum. Methods* **1989**, *B43*, 218.

(29) Maxwell, J. A.; Teesdale, W. J.; Campbell, J. L. *Nucl. Instrum. Methods* **1995**, *B95*, 407.

Received for review June 24, 1997. Revised manuscript received November 10, 1997. Accepted December 3, 1997.

ES9705553